

RSC Advances



This is an *Accepted Manuscript*, which has been through the Royal Society of Chemistry peer review process and has been accepted for publication.

Accepted Manuscripts are published online shortly after acceptance, before technical editing, formatting and proof reading. Using this free service, authors can make their results available to the community, in citable form, before we publish the edited article. This *Accepted Manuscript* will be replaced by the edited, formatted and paginated article as soon as this is available.

You can find more information about *Accepted Manuscripts* in the [Information for Authors](#).

Please note that technical editing may introduce minor changes to the text and/or graphics, which may alter content. The journal's standard [Terms & Conditions](#) and the [Ethical guidelines](#) still apply. In no event shall the Royal Society of Chemistry be held responsible for any errors or omissions in this *Accepted Manuscript* or any consequences arising from the use of any information it contains.

Cite this: DOI: 10.1039/c0xx00000x

www.rsc.org/xxxxxx

ARTICLE TYPE

Synthesis of hierarchical beta zeolite by using a bifunctional cationic polymer and the improved catalytic performance

Yangyang Yuan,^{a,b} Peng Tian,^a Miao Yang,^a Dong Fan,^{a,b} Linying Wang,^a Shutao Xu,^a Chan Wang,^{a,b} Dehua Wang,^{a,b} Yue Yang,^a Zhongmin Liu^{*a}

Received (in XXX, XXX) Xth XXXXXXXXX 20XX, Accepted Xth XXXXXXXXX 20XX

DOI: 10.1039/b000000x

Hierarchical beta zeolites have been hydrothermally synthesized by using commercial cationic polymer PDADMA as both microporogen and mesoporogen. The influence of various synthetic parameters on the products was systematically investigated. Products with narrow SiO₂/Al₂O₃ ratios were obtained under static crystallization conditions. By employing rotational condition and adding seeds in the initial gel, higher SiO₂/Al₂O₃ ratios over a wider range of 25 to 50 could be successfully achieved, which showed an obvious improvement. The ¹³C NMR, TG, XRF, N₂ sorption as well as molecular mechanics simulation results indicated that PDADMA was incorporated in the final product without decomposition, acting as a SDA for the formation of beta zeolite and mesoporogen simultaneously. Further studies on the crystallization process revealed that hierarchical structures templated by PDADMA had been formed in the early solid. The amorphous Si-Al species around the micropore channels gradually evolved to the beta structure under the assistance of PDADMA, whereas the mesopores formed at the initial period remained less changed. A solid-mediated mechanism is thus proposed for the synthesis. Characterization results showed that the obtained products had sphere-like morphology composed of 10-20 nm crystalline domains, high mesopore volumes, and large external surface areas. More importantly, the hierarchical beta zeolites exhibited greatly enhanced catalytic activity and stability in the cracking reaction of triisopropylbenzene.

1. Introduction

Zeolites are a family of crystalline aluminosilicates, which have been widely used as catalysts in the refining, petrochemical and fine chemical industries due to their uniform channels, large surface area and tunable acidity.¹⁻³ However, the relatively small micropore size of zeolites often brings diffusion limitation to the reaction involving bulky molecules, which can further cause negative effect on the activity, selectivity, and stability of the catalysts.⁴⁻⁷ Among the vast efforts made to enhance the mass transport in zeolites, creating mesopores in zeolite crystals has attracted great attention because it combines the advantages of mesoporous materials and zeolites.⁸⁻¹² Hitherto, various strategies have been developed for the preparation of hierarchical zeolites, including desilication or dealumination by post treatment^{13, 14} as well as through a hard-templating^{15, 16} or soft-templating route.¹⁷⁻²⁹

Direct hydrothermal synthesis of zeolites with mesoporosity is much interesting because it only involves a one-step procedure and can be easily scaled up. In addition, it may allow mesopore size adjustment while keeping the well integrity of the crystalline structure. Two general methodologies have been developed, including (i) dual templates strategy involving both micropore

structure-directing agent (SDA) and mesoporogen (surfactants, polymers, etc.);¹⁷⁻²⁷ (ii) bifunctional surfactant approach by using well-designed large molecule simultaneously containing micropore directing multi-ammonium heads and mesopore directing alkyl tails.^{28, 29} As to the first method, phase separation sometimes is observed with a mixture of zeolite crystals and mesoporous materials as the product. This is possibly due to the weaker interactions between the surfactant and the silicate species, and the mismatched crystallization rates associated with two templates. Using bifunctional structure-directing surfactant may be an effective way to avoid this problem. With this method, many zeolites with nanosheet or mesoporous structures have been synthesized.

Zeolite beta, with a three-dimensional interconnected pore system composed of 12-membered rings,³⁰ has exhibited excellent performance in hydroisomerization, hydrocracking, and alkylation.³¹⁻³³ Commercial beta zeolite is generally synthesized with expensive tetraethylammonium hydroxide (TEAOH) as the SDA. The hydrothermal synthesis of hierarchical beta has been explored by a number of works according to the methods mentioned above.²²⁻²⁶ Novel di-/multi-quaternary ammonium surfactants or compounds have been creatively synthesized and used as SDA to construct mesoporous beta.³⁴⁻³⁷ Unfortunately, most of the reported novel SDAs are commercially unavailable

and involve complex preparation process. It is highly desirable to develop a direct synthetic strategy by using a commercial and low cost template, which would benefit the industrial synthesis and application of hierarchical beta.

5 Herein, synthesis of hierarchical beta zeolite was realized by using a low-cost commercial cationic polymer polydiallyldimethylammonium chloride (PDADMA) as both microporogen and mesoporogen.³⁸ Cationic polymers, with high charge density and distinct properties from surfactants, have been reported as mesoporogen or dual-function SDA to prepare hierarchical zeolites. Xiao et al. first reported the use of mesoscale cationic polymer to produce hierarchical beta and ZSM-5.^{22,27,39} Afterwards, nanobeta aggregates with tunable mesopore size were realized by using cationic polymer as a flocculating agent.²⁶ Very recently, Xiao et al. synthesized hierarchical beta with SiO₂/Al₂O₃ ratios of 18-24 as a dual-function template and fumed silica as the Si source with cationic polymer PDADMA as a dual-function template.⁴⁰ In the present work, by using inexpensive silica sol as the Si source, mesoporous beta with tunable SiO₂/Al₂O₃ ratios (25-50), which is important for their catalytic applications, have been achieved with the help of PDADMA. The improved SiO₂/Al₂O₃ ratio should be due to the different Si sources (silica sol vs. fumed silica) and optimized synthetic conditions. The accelerated crystallization by a combination of seeds addition and rotational condition was believed to be the pivotal factor to obtain hierarchical beta with higher SiO₂/Al₂O₃ ratios. In addition, the influence of synthetic parameters on the products and the crystallization process were investigated in detail. 1,3,5-TIPB cracking reaction was selected as a probe reaction to test the catalytic performance of the products.

2. Experimental

2.1 Typical synthesis procedure for hierarchical beta

The chemical reagents used in the experiments include: NaAlO₂ (54.55 % Al₂O₃, 40.95 % Na₂O, Tianjin Guangfu Chemical Co.), colloidal silica (30.10% SiO₂, Qingdao Chengyu Chemical Co.), PDADMA (molecular weight: 600,000 g/mol, 40 % in water, Hangzhou Yinhu Chemical Co., Ltd.), NaOH (≥97 %, Tianjin Kemiou Chemical Reagent Co.), NH₄NO₃ (≥99 %, Tianjin Kemiou Chemical Reagent Co.), 1,3,5-triisopropylbenzene (≥95 %), and diallyl dimethyl ammonium chloride (60 % in water) bought from Aladdin Industrial Corporation. All the above reagents were used without further purification.

Typical synthesis of hierarchical beta zeolites under static condition: 2.08 g NaOH, 0.37 g NaAlO₂ and 58.00 g distilled water were mixed at room temperature, followed by the addition of 20.00 g colloidal silica under vigorous stirring. After 1 h of stirring, 6.00 g PDADMA was added to the gel, and then the resulting mixture was stirred vigorously for an additional 3 h to obtain a homogenous gel. The final mixture with a molar composition of 0.02Al₂O₃:1.00SiO₂:0.28Na₂O:40H₂O:0.14PDADMA (0.14 stands for the molar ratio of repeating unit in PDADMA) was transferred into a Teflon-lined stainless steel autoclave. The crystallization was carried out at 170 °C under static condition. The product was filtered, washed with distilled water, and dried at 100 °C for 12 h. The organic template in the

product was removed by calcination at 550 °C for 5 h. The proton forms of the samples were obtained by ion exchange with 1 M NH₄NO₃ aqueous solution (1g calcined sample in 10 ml solution) at 80 °C under stirring, and the solution was renewed every 2 h for three times. The solid was filtered, washed with deionized water, dried in air at 100 °C for 12 h, and calcined at 550 °C for 4 h.

Synthesis of hierarchical beta zeolite under rotational condition:

65 The synthesis procedure was similar to the above experiment except for the addition of beta seeds (as-synthesized sample 3 as seed, 5 wt% relative to SiO₂). The crystallization was carried out at 180 - 200 °C rotated at 60 rpm.

2.2 Characterization

70 The powder XRD pattern was recorded on a PANalytical X'Pert PRO X-ray diffractometer with Cu-Kα radiation (λ=0.15418 nm), operating at 40 kV and 40 mA. The chemical composition of the solid samples was determined with a Philips Magix-601 X-ray fluorescence (XRF) spectrometer. The crystal morphology was observed by scanning electron microscopy (Hitachi SU8020). Transmission electron microscopy (TEM) images were performed on a Tecnai G2 F20 S-TWIN microscope at an acceleration voltage of 200 kV. The sample was slightly ground before the TEM test. N₂ adsorption-desorption isotherms at -196 °C were determined on a Micromeritics ASAP 2020 system. Prior to the measurement, samples were degassed at 350 °C under vacuum for 5 h. The total surface area was calculated based on the BET equation. The micropore volume and micropore surface area were evaluated using the t-plot method. The mesopore size distribution was determined by the BJH method based on the adsorption branches of the isotherms. The liquid ¹³C NMR experiments were performed on a Bruker DRX-400 spectroscopy with a 5 mm probe. The chemical shifts were referenced to TMS. Solid state NMR experiments were performed on a Varian Infinity plus 400 WB spectrometer with BBO MAS probe operating at magnetic field strength of 9.4 T. The resonance frequencies were 104.2 and 79.4 MHz for ²⁷Al and ²⁹Si respectively. Chemical shifts were referenced to 1.0 M Al(NO₃)₃ for ²⁷Al and 2, 2-dimethyl-2-silapentane-5-sulfonate sodium salt (DSS) for ²⁹Si. The spinning rates of the samples at the magic angle were 4 and 6 kHz for ²⁷Al and ²⁹Si respectively. The thermal analysis was performed on a TA Q-600 analyzer with a temperature-programmed rate of 10 °C/min under an air flow of 100 ml/min. Temperature-programmed desorption of ammonia (NH₃-TPD) was measured on a chemical adsorption instrument of Micrometric 2920. Each sample (40-60 mesh, 0.15 g) was loaded into a stainless U-shaped micro reactor (i.d. = 5 mm) and pretreated at 600 °C for 1 h in flowing He. After the pretreatment, the sample was cooled down to 100 °C and saturated with NH₃ gas. Then, NH₃-TPD was carried out in a constant flow of He (20 ml/min) from 100 to 700 °C at a heating rate of 20 °C/min.

2.3 Catalytic reaction

1,3,5-triisopropylbenzene (TIPB) cracking was performed in a fixed-bed reactor at atmospheric pressure. 300 mg of the sample (40-60 mesh) was loaded into the reactor, and dehydrated in N₂ (50 ml/min) at 500 °C for 1 h prior to the reaction. The temperature of the catalytic bed was reduced to 230 °C in N₂ and

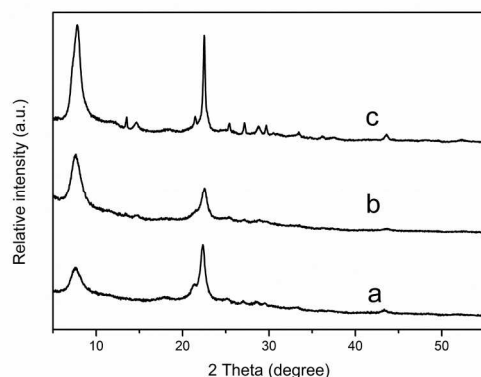


Fig. 1 XRD patterns of the as-synthesized sample 3 (a), calcined sample 3 (b) and commercial beta (c).

fed with vaporized TIPB (85 °C) in N₂ (50 ml/min). The products were analyzed on line by gas chromatography on an Agilent 6890 with an FID detector using a HP-5 column.

3. Results and discussion

3.1 Synthesis of hierarchical beta under static condition

The synthetic parameters for the hierarchical beta zeolites under static condition using PDADMA as a dual-functional porogen are summarized in Table 1. The X-ray diffraction (XRD) patterns of the products are presented in Fig. 1 and Fig. S1.

In the absence of PDADMA in the gel, mordenite with small quantity of quartz was formed as the solid product. Increasing the PDADMA/SiO₂ ratio to 0.105, the product became amorphous, indicating the inhibition effect of PDADMA on the crystallization of mordenite (MOR). Pure beta zeolite could be readily synthesized when the PDADMA/SiO₂ ratio reaches up to 0.140 or higher (samples 3-5). Notably, both the peak intensities and the height-to-width ratios in the XRD pattern of sample 3 are obviously lower than that of the commercial beta, suggesting the small crystal sizes of the present sample. The effect of Na₂O/SiO₂ ratio on the results was also investigated by fixing other synthetic conditions (samples 6-9). It turned out that the synthesis of beta zeolite was very sensitive to the alkaline amount in the initial gel. The ratio suitable for the formation of pure beta zeolite was limited in the range of $0.28 \leq \text{Na}_2\text{O}/\text{SiO}_2 < 0.32$. Lower Na₂O/SiO₂ ratio (0.25) greatly reduced the crystallization rate, whereas increasing the Na₂O/SiO₂ ratio in the gel up to 0.32 would cause the appearance of ANA phase. It should be noted that all the syntheses under static condition undergo long crystallization time (7-9 days). Possibly, the strong interactions between cationic polymer and negatively charged silica species slowed down the nucleation and growth rate. A detailed research on the crystallization process of beta zeolite would be given in the section below.

Preparation of hierarchical zeolites with adjustable SiO₂/Al₂O₃ ratio is always important, because it is closely related to their acidic/catalytic properties. Few reports on the synthesis of hierarchical beta pay attention to this issue, but more to the novelty of surfactant /compound porogens. Here, a series of experiments with different initial SiO₂/Al₂O₃ ratios were conducted at 170 °C under static condition (samples 10-12). As

Table 1 Gel compositions and products of the synthesis under static condition.^a

Sample	SiO ₂ /Al ₂ O ₃	Na ₂ O/SiO ₂	P/SiO ₂ ^b	t (day)	Product
1	50	0.28	0	7	MOR + Quartz
2	50	0.28	0.110	7	Amorphous
3	50	0.28	0.140	9	Beta
4	50	0.28	0.210	9	Beta
5	50	0.28	0.280	9	Beta
6	50	0.25	0.140	7	Amorphous + Beta
7	50	0.30	0.140	9	Beta
8	50	0.32	0.140	7	Beta + ANA
9	50	0.40	0.140	7	ANA
10	30	0.28	0.140	6.5	Beta + ANA
11	40	0.28	0.140	9	Beta + ANA
12	70	0.28	0.140	7	Beta + Kenyaite

^a Syntheses are carried out at 170 °C (H₂O/SiO₂ = 40 in the gel).

^b P/SiO₂ stands for the molar ratio of PDADMA repeating unit and SiO₂ in the gel.

can be seen, the SiO₂/Al₂O₃ ratio in the gel is almost unadjustable. Otherwise, ANA phase or kenyaite would appear as the impurity. This is in agreement with the report of Xiao et al. in which a narrow SiO₂/Al₂O₃ ratio has been found for PDADMA-templated beta zeolites.⁴⁰

3.2 Synthesis of hierarchical beta with higher SiO₂/Al₂O₃ ratio under rotational condition

During the exploration of synthesizing beta zeolite with higher SiO₂/Al₂O₃ ratio, we found that rotational crystallization assisted by the seeds could allow an obvious improvement. Detailed synthetic conditions are listed in Table 2. The XRD patterns of the as-synthesized products are shown in Fig. S2.

Pure beta zeolites (samples 13-15) were acquired from initial gels with SiO₂/Al₂O₃ ratios of 50-100 at 180 °C for 3 days. The corresponding SiO₂/Al₂O₃ ratio in the products showed an increase from 32.8 to 50.6 (Table 3). It suggests that rotational crystallization with the assistance of seeds can effectively inhibit

Table 2 Gel compositions and products of the synthesis under rotational condition with the addition of 5 % seed.

Sample	SiO ₂ /Al ₂ O ₃ ^a	Na ₂ O/SiO ₂	H ₂ O/SiO ₂	P/SiO ₂ ^b	T (°C)	t (day)	Product
13	50	0.28	40	0.14	180	3	Beta
14	75	0.28	20	0.14	180	3	Beta
15	100	0.28	20	0.14	180	3	Beta
16	50	0.28	40	0.14	190	1.5	Beta
17	50	0.28	40	0.14	200	2	Beta + FER+ Quartz

^a SiO₂/Al₂O₃ in the gel, not containing the compositions of the seed.

^b P/SiO₂ stands for the molar ratio of PDADMA repeating unit and SiO₂ in the gel.

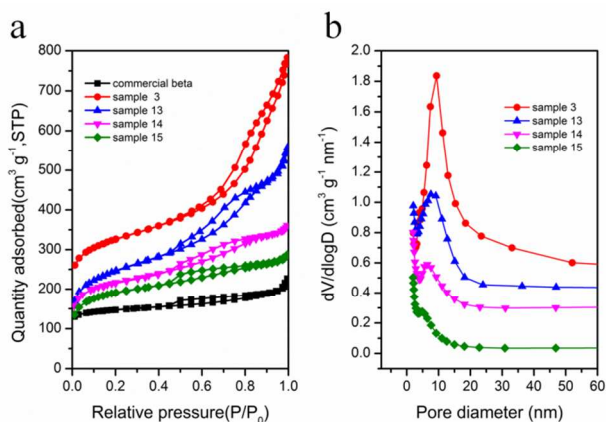


Fig. 2 N_2 adsorption-desorption isotherms (a) and pore size distribution curves from the adsorption branches (b) of the samples (the isotherms of sample 3 were vertically offset by $100 \text{ cm}^3 \text{ g}^{-1}$).

the formation of impurities in the product with higher $\text{SiO}_2/\text{Al}_2\text{O}_3$ ratio while accelerating the crystallization rate. The difference in the $\text{SiO}_2/\text{Al}_2\text{O}_3$ ratio between the gel and the product suggests that part of silica source is not involved in the formation of beta zeolite, in consistence with the observed solid yield of 45-55 % (calced basis). Moreover, it was found that the crystallization duration of the present system could be further shortened to 1.5 days by increasing the synthetic temperature to $190 \text{ }^\circ\text{C}$ (sample 16). At higher temperature, however, the product would become a mixture of beta, Fer and quartz (sample 17). Such a timesaving and low-cost approach for the facile preparation of hierarchical beta zeolites would be much attractive for their scale-up production and industrial applications.

3.3 Physicochemical properties of hierarchical beta zeolites

The N_2 adsorption-desorption isotherms of selected samples are presented in Fig. 2. The textural properties of the samples are summarized in Table 3. All the samples exhibit typical type-IV curves with an obvious increase at the relative pressure (P/P_0) of 0.40–0.90 due to the capillary condensation in the mesopores. The BJH pore-size distribution curves shown in Fig. 2b also confirm the mesopore systems in the synthesized products. Comparatively, the N_2 sorption isotherm of commercial sample has very small uptake at $0.2 < P/P_0 < 0.9$, corresponding to the small amount of mesoporosity.⁴¹ The total N_2 uptake of commercial sample is the lowest among the samples, suggesting its relatively low pore volume. As can be seen from Table 3, all beta products investigated present large external surface area and high mesopore volume in comparison with commercial sample. The mesopore volume of samples 3 and 13 reaches 0.94 and $0.72 \text{ cm}^3/\text{g}$ respectively, which is among the top ever reported for hierarchical zeolites. It should be mentioned that a decrease in mesopore volume and pore size distribution is observed for the products with higher $\text{SiO}_2/\text{Al}_2\text{O}_3$ ratios. Given that samples 14 and 15 have large external surface area of more than $300 \text{ m}^2/\text{g}$, it is supposed that the drop in mesopore volume is possibly due to the more closely packed nanocrystals.

The SEM images of hierarchical beta zeolites and commercial sample are shown in Fig. 3. Sample 3 synthesized under static condition shows spherical morphology with relatively uniform size of about 500-600 nm. Further magnification reveals that the spheres with non-smooth surface are composed of very small

Table 3 Chemical and textural properties of hierarchical beta and commercial beta samples

Sample	$\text{SiO}_2/\text{Al}_2\text{O}_3^a$	Surface area (m^2/g)			Pore volume (cm^3/g)	
		S_{BET}^b	S_{micro}^c	S_{external}^c	V_{micro}^c	V_{meso}^d
Commercial beta	23.9	497	381	115	0.17	0.17
3	29.3	789	316	473	0.14	0.94
13	32.8	862	331	532	0.15	0.72
14	37.3	727	383	344	0.18	0.37
15	50.6	661	336	325	0.15	0.27

^a Obtained by XRF (molar ratio). ^b BET surface area. ^c Micropore surface area, external surface area and micropore volume by t-plot method. ^d Mesopore volume by BJH method.

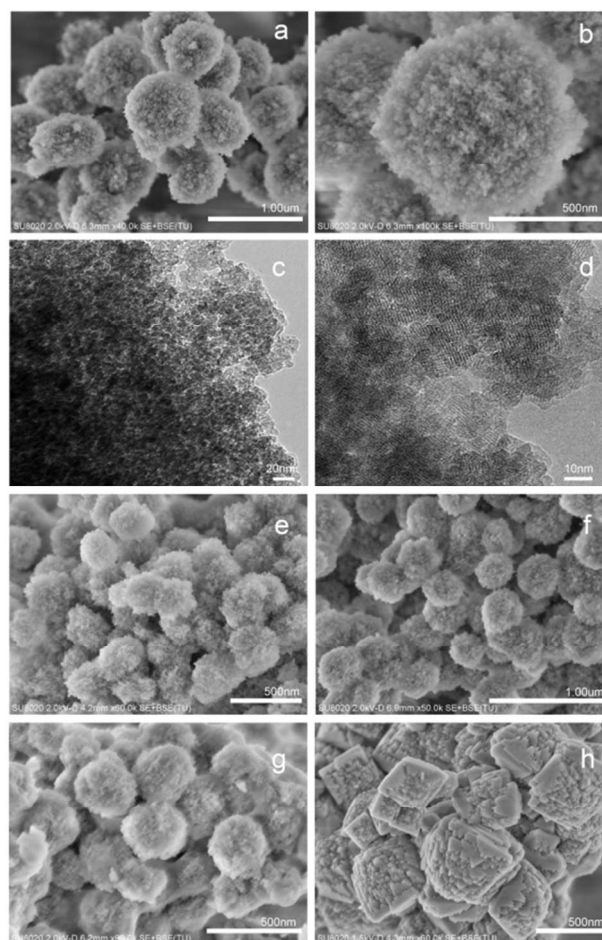


Fig. 3 SEM images of samples 3 (a, b), 13(e), 14 (f), 15(g), commercial beta (h) and TEM images of sample 3 (c, d).

particles. The morphology of samples obtained under rotational condition is similar to that of sample 3, but with smaller sphere size. In contrast, the commercial sample is comprised of relatively solid crystalline particles with crystal size ranging from 300 to 500 nm. The TEM images of sample 3 shown in Fig. 3 reveal that the spherical assembly is highly crystallized, which consists of nanocrystals of about 10-20 nm (only about 5-10 unit cells).⁴² The mesopores between the nanocrystals can be clearly observed, which are interconnected and open to the external

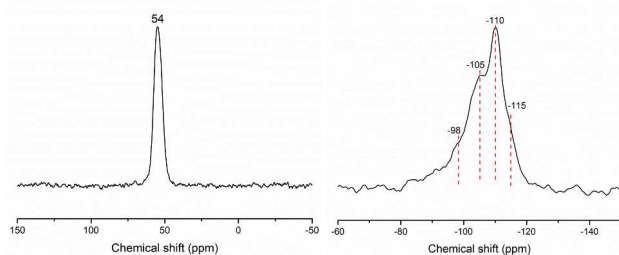


Fig. 4 ^{27}Al and ^{29}Si MAS NMR spectra of the as-synthesized beta (sample 3)

surface of the particles. Therefore, the small particle size results in the increase of the external surface area and nanocrystals together with their interconnection ensure the high mesopore volume,⁴³ in good agreement with the results of N_2 sorption. The large proportion of acid sites on external surface would be beneficial for reactions involving bulky molecules. In addition, the smaller crystal size could greatly shorten the diffusion length compared with conventional zeolites.

Fig. 4a displays the ^{27}Al MAS NMR spectrum of the as-synthesized beta product (sample 3). There only exists one peak centered at 54 ppm, arising from the tetrahedral aluminum species. The ^{29}Si MAS NMR spectrum of the same sample is shown in Fig. 4b. One strong resonance at -110 ppm together with three shoulders at -115 ppm, -105 ppm and -98 ppm can be observed. According to the literatures, the peak at -115 and -110 ppm are ascribed to $\text{Si}(0\text{Al})$ species and the peak at -105 ppm corresponds to $\text{Si}(1\text{Al})$ species.⁴⁴ The small shoulder centered at -98 ppm is assigned to $\text{Si}(\text{OH})$ species in the defect sites. The corresponding $\text{SiO}_2/\text{Al}_2\text{O}_3$ ratio calculated based on the ^{29}Si NMR spectrum is 29.8, in accordance with the XRF result.

Thermal analysis (TG-DSC) was carried out to investigate the content of the organic template in the product (sample 3). The results are shown in Fig. S3. Two weight losses could be clearly observed in the TG curve (sample 3). The first weight loss about 7 % in the temperature range of 0-200 °C with an endothermic effect is due to the removal of water from the zeolites. The second weight loss of 33 % in the temperature range of 200-650 °C with exothermic effect is attributed to the combustion removal of the cationic polymer. Such a high weight loss is consistent with the large mesopore volume of the sample.

^{13}C NMR spectra were employed to investigate the status of organic polymer in the as-synthesized hierarchical product (Fig. S4). The spectrum of the liquid obtained by dissolving as-synthesized sample 3 in HF solution is similar to that of PDADMA solution, suggesting the intactness of the polymer during crystallization. In order to further understand the templating role of PDADMA, control syntheses without the use of PDADMA or using the cationic monomer (dimethyl diallyl ammonium chloride) as a SDA were conducted, but failed with a mixture of mordenite and quartz as the final products. It seems that the 5-membered cyclic quaternary ammonium cation in the polymer chain is important for the formation of beta structure.

Using polymer containing ten repeating units as the model compound, the geometrical optimization by molecular mechanics simulation was performed (Fig. 5). The maximum dimension of a repeating unit is calculated to be 0.65×0.42 nm, which is close to the pore sizes of beta zeolites (0.66×0.67 nm and 0.56×0.56 nm

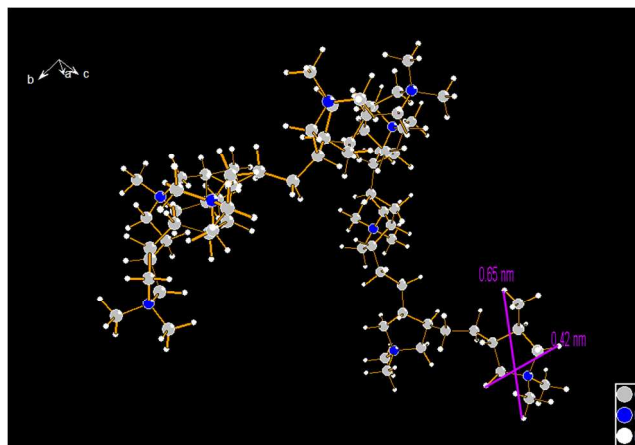


Fig. 5 The optimal geometry conformation of PDADMA molecule (10-unit) determined using molecular mechanics simulation method employing the Forcite module embedded in the Material Studio 6.0 software.

in the [100] and [001] direction, respectively). It is thus speculated that the polymer chain locates within the 12-membered rings along the direction of the channels. However, not the entire polymer chain is expected to be occluded in the channel because of its extreme length (the calculated chain length would be 2.4 μm for PDADMA with a molecular weight of 6×10^5 g/mol). The rest part of the chain outside the micropore of beta zeolite would have strong interaction with the negatively charged crystal surface (resulting from the alkaline media) due to its highly positive charge density. This electrostatic interaction would prevent the further growth of the crystal and result in the hierarchical structure. To further verify the speculation, N_2 sorption on the as-synthesized sample (Fig. S5) was performed, which gives a type-IV isotherm. The absence of micropore volume and lower mesopore volume ($0.30 \text{ cm}^3/\text{g}$) as compared with that of calcined one indicates the total occupation of the polymer in the micropores and partial occupation in the mesopores,⁴⁵ confirming our speculation well. In addition, based on the XRF results that only small amount of sodium and chlorine existed in the as-synthesized sample 3 (Cl 0.036wt%, $\text{Na}/\text{Al}=0.034$ in mole, the sample had been carefully washed), it confirmed that the polymer acted as the main SDA for the formation of beta zeolite, though the Na^+ was indispensable for the synthesis as shown in the above (Table 1 and 2). Na^+ may serve as a co-SDA together with the cationic polymer during the synthesis, but it only occupies a very small proportion.

3.4 Investigation of the crystallization process

In order to understand the growth process of hierarchical beta, samples with different crystallization time were investigated (the initial gel has the same molar composition as that of sample 3). The XRD patterns (Fig. 6) reveal the evolution of long-range order of the samples. No apparent diffraction peak was observed in the XRD pattern of the 1 d sample, indicating the amorphous characteristic. After 3 days, very weak diffraction peaks at 7.6° and 22.3° began to appear, which suggests the formation of small amount of beta zeolite. Subsequently, the peak intensities gradually increased with time and well-defined diffraction pattern could be obtained after 9 days. The SEM images (Fig. 7) indicated that there only existed irregular agglomerates in the 1 d

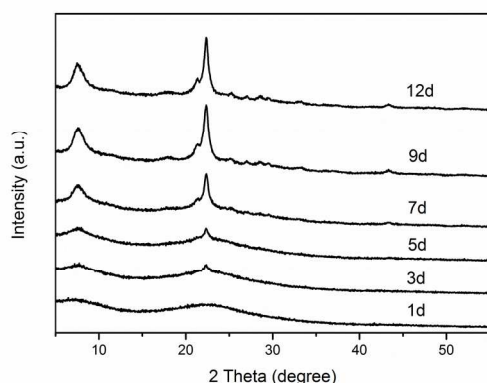


Fig. 6 XRD patterns of the as-synthesized samples with different crystallization times (The initial gel has the same molar composition as that of sample 3)

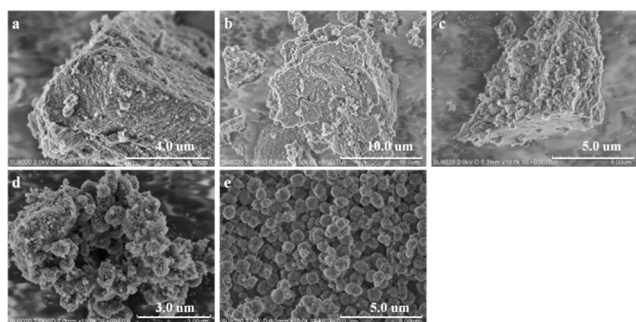


Fig. 7 SEM images of the samples with different crystallization time: (a) 1 day, (b) 3 day, (c) 5 day, (d) 7 day, (e) 9 day.

sample. After heating for 3 d, less change could be found in spite of the presence of weak peaks in the XRD pattern. With the hydrothermal treatment time prolonging to 5 days, small amount of sphere-like crystals could be distinguished at the surface of amorphous materials. Afterwards, more sphere particles with diameter of about 500 nm formed, which closely connected with the residue amorphous materials. Finally, only pure beta crystallites could be observed in the 9 d sample.

The N_2 sorption analyses of the samples were performed to monitor the evolution of the porosity during the crystallization process (Fig. S6 and Table 4). Interestingly, porous structures have already been generated in the 1 d sample with a micropore and mesopore volume of 0.06 and 0.68 cm^3/g , respectively. The presence of large mesopore volume is understandable, owing to the removal of entrapped polymer. But it is somewhat unexpected to see the creation of the microporosity in this early amorphous solid. Further analyzing the pore size distribution (Fig. S7)

Table 4. Chemical compositions and textural properties of the samples with different crystallization time.^a

Sample	SiO_2/Al_2O_3 ^b	Yield (%)	S_{BET} ^c (m^2/g)	S_{micro} ^d (m^2/g)	$S_{external}$ ^d (m^2/g)	V_{micro} ^d (cm^3/g)	V_{meso} ^c (cm^3/g)
1d	29.8	47%	448	151	297	0.06	0.68
3d	29.4	47%	492	160	332	0.07	0.78
5d	29.5	49%	485	161	323	0.07	0.73
7d	29.5	49%	688	250	437	0.11	0.93
9d	29.3	48%	789	316	473	0.14	0.94

^a The initial gel has the same molar composition as that of sample 3. ^b Obtained by XRF (molar ratio). ^c BET surface area. ^d Micropore area, external surface area and micropore volume by t-plot method. ^e Mesopore volume by BJH method.

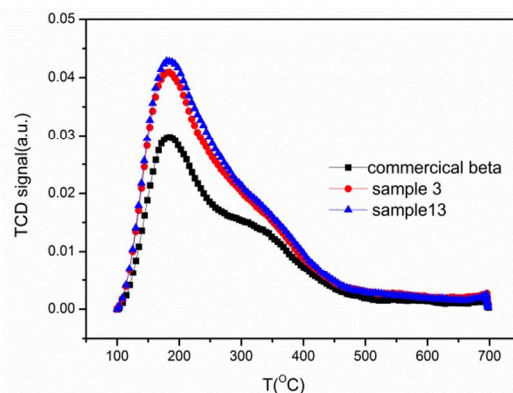


Fig. 8 NH_3 -TPD curves of sample 3, sample 13 and commercial beta

reveals that the micropore aperture of the 1 d sample is different from that of the final beta product. The former is obviously larger than the latter. Following the formation of hierarchical beta as evidenced by XRD and SEM, both the microporosity and mesoporosity of the samples showed an increasing trend with time and reached their maximum at 9 days. It should be mentioned that the mesopores centred around 14 nm in the solid samples remained almost unaltered during the whole synthesis course. These results demonstrate that PDADMA has strong micropore-directing ability in the present system, which plays the role of microporogen and mesoporogen since the initial period of the crystallization. The amorphous Si-Al species around the micropore channels of the initial solid could evolve to uniform beta structure under the assistance of PDADMA, whereas the mesopores formed by PDADMA at the initial period remained less changed. In addition, it was found that the SiO_2/Al_2O_3 ratios of the samples and the solid yields kept close to each other during the crystallization (Table 4). We thus suggest that a solid-mediated mechanism may occur during the crystallization of hierarchical beta.^{46,47}

3.5 Surface acidity and catalytic performance of hierarchical beta zeolite

The NH_3 -TPD experiment was carried out to investigate the acid properties of the protonated hierarchical beta and commercial sample. As shown in Fig. 8, all profiles exhibit two peaks centered at 182 °C and 345 °C. The low-temperature peak is assigned to ammonia desorbed from the weak acid site and the high-temperature peak corresponds to desorption from the strong acid sites. In comparison with the commercial sample, both hierarchical beta zeolites (samples 3 and 13) showed a

Cite this: DOI: 10.1039/c0xx00000x

www.rsc.org/xxxxxx

ARTICLE TYPE

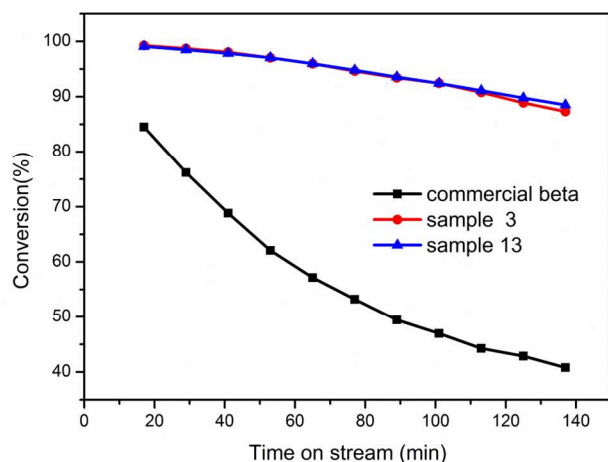


Fig. 9 Catalytic cracking conversion of 1,3,5-triisopropylbenzene (TIPB) over hierarchical beta and commercial beta. Reaction conditions: vaporized TIPB in nitrogen (50 ml/min, 85 °C) as feed, reaction temperature: 230 °C, catalyst: 0.3 g.

considerable improvement in the weak acid concentration and slight increase in the strong acid concentration. Since sample 3 and 13 possessed slightly higher $\text{SiO}_2/\text{Al}_2\text{O}_3$ ratios than the commercial sample, the improved acid concentration of hierarchical samples may reflect the distinct Al location/distribution associated with the use of polymer and would benefit their catalytic applications.⁴⁸

The catalytic performance of the hierarchical samples was investigated by the reaction involving bulky organic molecules. The abundant mesoporosity and large external surface area are believed to facilitate the diffusion and the improvement of the catalyst activity and stability. Herein, the cracking of 1, 3, 5-triisopropylbenzene was used as a probe reaction. Both Brønsted and Lewis acid sites are active for the TIPB cracking.^{49, 50} For zeolite catalysts, the cracking activity is generally related to the Brønsted acidity.⁵¹ Given that the kinetic molecular dimension of TIPB (about 0.95 nm) is larger than the micropore size of the beta, the effective catalytic sites for the cracking should be mainly from the external surface of the catalysts (the acid sites in the micropores may contribute to the deep cracking such as cumene to benzene).⁵²

As shown in Fig. 9, both hierarchical beta zeolites displayed not only higher activity, but also much better stability. Under the investigated conditions, a 99% conversion of TIPB was achieved with hierarchical catalysts at the initial reaction, whereas 85% conversion obtained over the commercial one. Subsequently, commercial sample suffered from fast deactivation and the conversion of TIPB decreases to 39.6% at TOS of 137 min. The hierarchical samples showed less deactivation and the conversion of TIPB maintains at 90% at this time. In combination with the above results of textural property and acidity characterization, the good catalytic activities and stabilities of hierarchical samples

should be attributed to their abundant mesoporosity and small crystal size, which increases the accessibility of reactants to the acid sites and facilitate the product diffusion.⁵⁰

4 Conclusions

In the present work, we synthesized hierarchical beta zeolite with low-cost commercial polymer PDADMA as a bifunctional porogen. The fastened crystallization process assisted by the seeds addition under rotational condition was found to be crucial to acquire hierarchical beta over a wider range of $\text{SiO}_2/\text{Al}_2\text{O}_3$ ratios. The $\text{SiO}_2/\text{Al}_2\text{O}_3$ ratios in the products could be tuned from 25 to 50, which are higher than the ratio of 18-24 achieved with the same polymer reported recently. This is also important for their catalytic applications. Investigation on the crystallization process revealed a solid-mediated mechanism for the present synthesis. Characterization results indicated that PDADMA served as the main SDA for the formation of beta structure and the products assembled by small zeolite crystallites (10-20 nm) featured very high surface areas and large mesopore volumes. The hierarchical beta zeolites exhibited excellent activity and stability in the cracking reaction of TIPB as compared to conventional sample. It is expected that this facile approach, taking advantage of low cost and tunable $\text{SiO}_2/\text{Al}_2\text{O}_3$ ratios, could bring new possibilities for the scale-up synthesis and industrial applications of hierarchical beta zeolite. In the future, exploration on the micropore-directing ability of cationic polymers to other kinds of zeolites would also be necessary.

Acknowledgements

The authors would like to acknowledge the National Natural Science Foundation of China (Grant no. 21101150, Grant no.21103180 and Grant no.21473182) for the support of this project.

Notes and references

1. A. Corma, *Chem. Rev.*, 1997, **97**, 2373-2419.
2. J. Weitkamp, *Solid State Ionics* 2000, **131**, 175-188.
3. C. S. Cundy and P. A. Cox, *Chem. Rev.*, 2003, **103**, 663-701.
4. M. E. Davis, *Nature*, 2002, **417**, 813-821.
5. G. Q. Guo, H. Chen and Y. C. Long, *Microporous Mesoporous Mater.*, 2000, **39**, 149-161.
6. I. Fechete, P. Caullet, E. Dumitriu, V. Hulea and H. Kessler, *Appl. Catal., A*, 2005, **280**, 245-254.
7. D. Prochazkova, L. Kurfirtova and J. Pavlatova, *Catal. Today* 2012, **179**, 78-84.
8. M. Hartmann, *Angew. Chem. Int. Ed.*, 2004, **43**, 5880-5882.
9. L. H. Chen, X. Y. Li, J. C. Rooke, Y. H. Zhang, X. Y. Yang, Y. Tang, F. S. Xiao and B. L. Su, *J. Mater. Chem.*, 2012, **22**, 17381-17403.
10. K. Na, M. Choi and R. Ryoo, *Microporous Mesoporous Mater.*, 2013, **166**, 3-19.
11. K. Moller and T. Bein, *Chem. Soc. Rev.*, 2013, **42**, 3689-3707.

12. M. Milina, S. Mitchell, P. Crivelli, D. Cooke and J. Perez-Ramirez, *Nat. Commun.*, 2014, **5**.
13. D. Verboekend, M. Milina, S. Mitchell and J. Perez-Ramirez, *Cryst. Growth Des.*, 2013, **13**, 5025-5035.
14. S. K. Saxena, N. Viswanadham and T. Sharma, *J. Mater. Chem.*, 2014, **2**, 2487-2490.
15. Y. S. Tao, H. Kanoh and K. Kaneko, *J. Am. Chem. Soc.*, 2003, **125**, 6044-6045.
16. C. Sun, J. M. Du, J. Liu, Y. S. Yang, N. Ren, W. Shen, H. L. Xu and Y. Tang, *Chem. Commun.*, 2010, **46**, 2671-2673.
17. M. Choi, H. S. Cho, R. Srivastava, C. Venkatesan, D. H. Choi and R. Ryoo, *Nat. Mater.*, 2006, **5**, 718-723.
18. L. L. Wu, V. Degirmenci, P. C. M. M. Magusin, B. M. Szyja and E. J. M. Hensen, *Chem. Commun.*, 2012, **48**, 9492-9494.
19. Y. Zhu, Z. Hua, X. Zhou, Y. Song, Y. Gong, J. Zhou, J. Zhao and J. Shi, *RSC Adv.*, 2013, **3**, 4193-4198.
20. D. Nandan, S. K. Saxena and N. Viswanadham, *J. Mater. Chem.*, 2014, **2**, 1054-1059.
21. Q. Y. Wang, S. T. Xu, J. R. Chen, Y. X. Wei, J. Z. Li, D. Fan, Z. X. Yu, Y. Qi, Y. L. He, S. L. Xu, C. Y. Yuan, Y. Zhou, J. B. Wang, M. Z. Zhang, B. L. Su and Z. M. Liu, *RSC Adv.*, 2014, **4**, 21479-21491.
22. F. S. Xiao, L. F. Wang, C. Y. Yin, K. F. Lin, Y. Di, J. X. Li, R. R. Xu, D. S. Su, R. Schlogl, T. Yokoi and T. Tatsumi, *Angew. Chem. Int. Ed.*, 2006, **45**, 3090-3093.
23. J. Aguadoa, D. P. Serrano and J. M. Rodriguez, *Microporous Mesoporous Mater.*, 2008, **115**, 504-513.
24. H. Zhu, Z. Liu, D. Kong, Y. Wang and Z. Xie, *J. Phys. Chem. C* 2008, **112**, 17257-17264.
25. L. J. Liu, H. B. Wang, R. W. Wang, S. J. Zeng, L. Ni, D. L. Zhang, L. K. Zhu, H. B. Zou, S. L. Qiu and Z. T. Zhang, *RSC Adv.*, 2014, **4**, 39297-39300.
26. K. Möller, B. Yilmaz, U. Mueller and T. Beins, *Chem. Mater.*, 2011, **23**, 4301-4310.
27. F. J. Liu, T. Willhammar, L. Wang, L. F. Zhu, Q. Sun, X. J. Meng, W. Carrillo-Cabrera, X. D. Zou and F. S. Xiao, *J. Am. Chem. Soc.*, 2012, **134**, 4557-4560.
28. M. Choi, K. Na, J. Kim, Y. Sakamoto, O. Terasaki and R. Ryoo, *Nature*, 2009, **461**, 246-U120.
29. K. Na, C. Jo, J. Kim, K. Cho, J. Jung, Y. Seo, R. J. Messinger, B. F. Chmelka and R. Ryoo, *Science*, 2011, **333**, 328-332.
30. J. M. Newsam, M. M. J. Treacy, W. T. Koetsier and C. B. Degruyter, *Proc. R. Soc. London, Ser. A*, 1988, **420**, 375-405.
31. G. Bellussi, G. Pazzuconi, C. Perego, G. Girotti and G. Terzoni, *J. Catal.*, 1995, **157**, 227-234.
32. A. Hassan, S. Ahmed, M. A. Ali, H. Hamid and T. Inui, *Appl. Catal., A*, 2001, **220**, 59-68.
33. A. Martins, J. M. Silva and M. F. Ribeiro, *Appl. Catal., A*, 2013, **466**, 293-299.
34. B. Liu, Y. Tan, Y. Ren, C. Li, H. Xi and Y. Qian, *J. Mater. Chem.*, 2012, **22**, 18631-18638.
35. R. Kore, B. Satpati and R. Srivastava, *Chem. Eur. J.*, 2011, **17**, 14360-14365.
36. K. Cho, K. Na, J. Kim, O. Terasaki and R. Ryoo, *Chem. Mater.*, 2012, **24**, 2733-2738.
37. R. Kore, R. Sridharkrishna and R. Srivastava, *RSC Adv.*, 2013, **3**, 1317-1322.
38. Y. Y. Yuan, P. Tian, Z. M. Liu, M. Yang, L. Y. Wang and Y. Zhang, China Patent, Application Number: 201310369527.7.
39. J. Song, L. Ren, C. Yin, Y. Ji, Z. Wu, J. Li and F.-S. Xiao, *J. Phys. Chem. C* 2008, **112**, 8609-8613.
40. J. Zhu, Y. Zhu, L. Zhu, M. Rigutto, A. van der Made, C. Yang, S. Pan, L. Wang, L. Zhu, Y. Jin, Q. Sun, Q. Wu, X. Meng, D. Zhang, Y. Han, J. Li, Y. Chu, A. Zheng, S. Qiu, X. Zheng and F.-S. Xiao, *J. Am. Chem. Soc.*, 2014, **136**, 2503-2510.
41. Y. Kalvachev, M. Jaber, V. Mavrodinova, L. Dimitrov, D. Nihtianova and V. Valtchev, *Microporous Mesoporous Mater.*, 2013, **177**, 127-134.
42. K. Möller, B. Yilmaz, R. M. Jacubinas, U. Müller and T. Bein, *J. Am. Chem. Soc.*, 2011, **133**, 5284-5295.
43. L. Tosheva and V. P. Valtchev, *Chem. Mater.*, 2005, **17**, 2494-2513.
44. S. Mintova, V. Valtchev, T. Onfroy, C. Marichal, H. Knozinger and T. Bein, *Microporous Mesoporous Mater.*, 2006, **90**, 237-245.
45. L. F. Zhu, L. M. Ren, S. J. Zeng, C. G. Yang, H. Y. Zhang, X. J. Meng, M. Rigutto, A. van der Made and F. S. Xiao, *Chem. Commun.*, 2013, **49**, 10495-10497.
46. W. Y. Xu, J. Q. Li, W. Y. Li, H. M. Zhang and B. C. Liang, *Zeolites*, 1989, **9**, 468-473.
47. D. P. Serrano, M. A. Uguina, G. Ovejero, R. VanGrieken and M. Camacho, *Microporous Mater.*, 1996, **7**, 309-321.
48. J. Dědeček, Z. Sobalík and B. Wichterlová, *Cat. Rev. - Sci. Eng.*, 2012, **54**, 135-223.
49. K. Roos, A. Liepold, H. Koch and W. Reschtilowski, *Chem.Eng.Technol.*, 1997, **20**, 326-332.
50. K. A. Mahgoub and S. Al-Khattaf, *Energy & Fuels*, 2005, **19**, 329-338.
51. S. Schallmoser, T. Ikuno, M. F. Wagenhofer, R. Kolvenbach, G. L. Haller, M. Sanchez-Sanchez and J. A. Lercher, *J. Catal.*, 2014, **316**, 93-102.
52. J. A. Zhou, Z. L. Hua, Z. C. Liu, W. Wu, Y. Zhu and J. L. Shi, *Acc Catal.*, 2011, **1**, 287-291.

^aNational Engineering Laboratory for Methanol to Olefins, Dalian National Laboratory for Clean Energy, Dalian Institute of Chemical Physics, Chinese Academy of Sciences, Dalian 116023, P. R. China; *E-mail: liuzm@dicp.ac.cn. ^bUniversity of Chinese Academy of Sciences, Beijing, P. R. China

†Electronic Supplementary Information (ESI) available: More details of characterization data. See DOI:10.1039/b000000x/.